remote sensing

MDPI

Article

Delineating Spatial Patterns in Human Settlements Using VIIRS Nighttime Light Data: A Watershed-Based Partition Approach

Ting Ma [1,2,3,*], Zhan Yin [1,2] and Alicia Zhou [4]

1 State Key Laboratory of Resources and Environmental Information System, Institute of Geographical Sciences and Natural Resources Research, Chinese Academy of Sciences, Beijing 100101, China; yinz@lreis.ac.cn
2 University of Chinese Academy of Sciences, Beijing 100049, China
3 Jiangsu Center for Collaborative Innovation in Geographical Information Resource Development and Application, Nanjing 210023, China
4 Department of Mathematics & Statistics, College of Art and Science, Boston University, Boston, MA 02215, USA; azhou96@bu.edu
* Correspondence: mting@lreis.ac.cn; Tel.: +86-10-6488-9769

Received: 7 February 2018; Accepted: 14 March 2018; Published: 15 March 2018

Abstract: As an informative proxy measure for a range of urbanization and socioeconomic variables, satellite-derived nighttime light data have been widely used to investigate diverse anthropogenic activities in human settlements over time and space from the regional to the national scale. With a higher spatial resolution and fewer over-glow and saturation effects, nighttime light data derived from the Visible Infrared Imaging Radiometer Suite (VIIRS) instrument with day/night band (DNB), which is on the Suomi National Polar-Orbiting Partnership satellite (Suomi-NPP), may further improve our understanding of spatiotemporal dynamics and socioeconomic activities, particularly at the local scale. Capturing and identifying spatial patterns in human settlements from VIIRS images, however, is still challenging due to the lack of spatially explicit texture characteristics, which are usually crucial for general image classification methods. In this study, we propose a watershed-based partition approach by combining a second order exponential decay model for the spatial delineation of human settlements with VIIRS-derived nighttime light images. Our method spatially partitions the human settlement into five different types of sub-regions: high, medium-high, medium, medium-low and low lighting areas with different degrees of human activity. This is primarily based on the local coverage of locally maximum radiance signals (watershed-based) and the rank and magnitude of the nocturnal radiance signal across the whole region, as well as remotely sensed building density data and social media-derived human activity information. The comparison results for the relationship between sub-regions with various density nighttime brightness levels and human activities, as well as the densities of different types of interest points (POIs), show that our method can distinctly identify various degrees of human activity based on artificial nighttime radiance and ancillary data. Furthermore, the analysis results across 99 cities in 10 urban agglomerations in China reveal inter-regional variations in partition thresholds and human settlement patterns related to the urban size and form. Our partition method and relative results can provide insight into the further application of VIIRS DNB nighttime light data in spatially delineated urbanization processes and socioeconomic activities in human settlements.

Keywords: nighttime light; Suomi-NPP VIIRS; human settlement; watershed-based partition; second-order exponential decay

1. Introduction

As a human-dominated landscape, human settlements ranging in size from hamlets and villages to towns and cities play a crucial role in environmental and ecological changes [1–3]. Understanding human settlement patterns, therefore, is important for a range of issues, such as city planning, environmental conservation, resource sustainability and political decision-making [4–6]. Based on the statistically significant relationship between nocturnal artificial lighting signals and several urbanization and socioeconomic variables over time and space [7,8], satellite-derived nighttime light data, which were previously provided by the Defense Meteorological Satellite Program (DMSP), have been widely applied when investigating socioeconomic dynamics and mapping urbanization at various spatial and temporal scales [9–12]. The most notable advantage of nighttime light images is that they can provide timely and consistent observations of socioeconomic dynamics with spatially explicit characteristics and spatially represent a variety of information for human activities when compared to traditional statistical data and visible and near-infrared remote sensing data, respectively [13]. In practice, however, DMSP nighttime light datasets have several considerable drawbacks due to factors such as a relatively coarse spatial resolution, saturated lighting signals due to the limited capability of the six-bit quantization sensors and over-glow effects caused by light diffusion from adjacent areas, which can visibly affect the quantitative measurement of human activities, particularly at a fine scale [14,15]. Thus, most previous studies based on DMSP nighttime light data have generally been limited to regional or sub-regional level surveys of urbanization dynamics and socioeconomic development, even though several efforts have been made to calibrate radiance values and reduce saturation effects in DMSP images [16–18].

Recent global composites of nighttime light images, which have been derived from the Visible Infrared Imaging Radiometer Suite (VIIRS) instrument day/night band (DNB) since 2012 [19], show an unprecedented and detailed look at human settlements due to a wider range of radiometric detection, a higher spatial resolution and fewer over-glow effects compared to the DMSP data [20–22]. Hence, VIIRS nighttime light datasets might have great potential for the detailed characterization of human settlements with various socioeconomic activities at a fine scale [23,24]. Several studies have demonstrated that VIIRS images can generate more accurate measures of regional socioeconomic variables [25–27], as well as the spatial extent of urbanized land [28].

Apart from regional-level investigations of the quantitative responses of nighttime lighting signals to various urbanization parameters and socioeconomic variables, many efforts have been made to develop applicable nighttime light data methods to extract urbanized land features from both DMSP and VIIRS images [29–33]. Dou et al. [34] summarized these methods into three different categories: thresholding, a composite index and supervised classification. Examples of the recent use of these methods mainly include local-optimized thresholding (LOT), the vegetation-adjusted nighttime light urban index (VANUI) and support vector machine classification (INNL-SVM). For the most part, these methods mainly focus on the automatic extraction of the spatial extent of urban built-up areas that closely match the statistical data or the mapping results of high spatial resolution images. Ma et al. [35] proposed a pixel-level approach based on the quadratic relationship between nocturnal radiance values and the brightness gradient to partition DMSP nighttime light images into five types of lighting areas for individual cities. Each type of identified area can be associated with specified subareas of human settlement, with various forms and human activities. However, this partition method might not be applicable to VIIRS data because increased spatial fluctuations in radiance values at a relatively fine scale may not support the robust quadratic relationship.

Further applications of nightlight imagery, particularly when investigating human settlement patterns at the local scale, are still less documented and are a challenge, which is largely due to the lack of partition approaches for delineating the spatial features of artificial landscapes from nighttime light images. Although both remotely sensed DMSP and VIIRS images provide us with an efficient way to survey the overall degree of regional socioeconomic activities through anthropogenic nightlight emissions, it is hardly possible to produce spatially explicit classifications of the land cover feature

composite from nocturnal brightness signals without connections to spectral and texture characteristics of lit artificial objects. Hence, a spatially explicit partition method is required for delineating human settlements using nighttime light images. Moreover, an association between nightlight signals and social media-derived information can further improve our understandings of spatial patterns in demographic and socioeconomic activities [36–38].

The primary objective of this study is to develop a spatial partition approach to identify different types of lit areas in human settlements from VIIRS nighttime light images. Our method is primarily derived from a watershed concept, which is based on local lighting hotspots and identifies adjacent units like a topographic map, with a second order exponential decay model which is used for measuring changes in brightness with respect to the rank among different partitioned units. Satellite-derived building density data and social media-based human activity information are jointly used to further identify partitioned sub-regions into different types of lighting areas. Based on nightlight watershed unit, the utility of the watershed-based approach for delineating human settlement patterns is demonstrated using points of interest (POI) data to represent various settlement types at the local scale, and further applications of our method for delineating human settlements are carried out for 99 cities in 10 urban agglomerations.

2. Materials and Methods

2.1. VIIRS Nighttime Light Data

The monthly composite of VIIRS nighttime light images (January 2016) used in this study (see Figure 1a) is provided by NOAA's National Centers for Environmental Information (NCEI) (the data were downloaded from https://ngdc.noaa.gov/eog/viirs/index.html). Current VIIRS monthly composite images are produced in 15 arc-seconds (~500 m at the equator) geographic grids, where the effects of the aurora, fires, boats, and other ephemeral lights have not been removed [39]. To reduce the effect of unstable nighttime lighting sources and background noise, we ensure the following: (1) the maximum radiance value of nighttime light (NTL, which is 290 nano Watt cm^{-2} sr^{-1} in this study) derived from three well-developed cities (Beijing, Shanghai and Guangzhou), which are highly intensified human settlements was selected to be the upper threshold; (2) all gridded pixels with an initial radiance exceeding the upper threshold of NTL were replaced correspondingly; and (3) the DMSP composite of annual stable nighttime light, with a digital number larger than zero in 2013, was used as an image mask to filter the background noise of the VIIRS image.

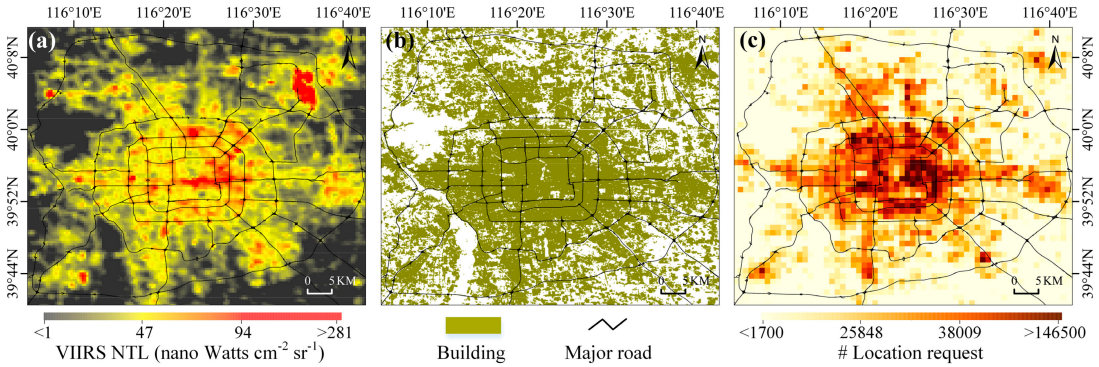

Figure 1. Examples of multiple data sources over the city of Beijing. (**a**) Visible Infrared Imaging Radiometer Suite (VIIRS)-derived nighttime brightness data; (**b**) Global Urban Footprint (GUF)-derived artificial building areas; (**c**) The number of location requests derived from Tencent's big data platform.

2.2. Ancillary Data

A satellite-based binary settlement dataset representing built-up and non-built-up areas was derived from Global Urban Footprint (GUF) products provided by the German Remote Sensing Data Center (DFD) of the German Aerospace Center (DLR). GUF global human settlement images [40] (available at https://geoservice.dlr.de/web/maps/eoc:guf:3857) were originally collected by very high-resolution synthetic aperture radars between 2011 and 2013 and processed into final identified images of highly structured and heterogeneous built-up areas, with a spatial resolution of ~3 arc-seconds (~84 m at the equator) (see Figure 1b). The social media-derived data, which represent the aggregated amount of location requests sent by anonymous users for diverse location-awareness services (e.g., navigating, location sharing and exploring nearby areas), are collected from the Tencent's big data location database (over the period 16 January to 13 February 2016, available at https://heat.qq.com), which is the largest Chinese social media platform. Gridded Tencent data provide a representative estimation of the total degree of human activity at the grid cell-level [41], with a spatial resolution of ~1 km by 1 km (see Figure 1c). In this study, GUF and Tencent data are used to investigate the density of built-up areas and the magnitude of human activities, respectively, for sub-regions that are initially partitioned by VIIRS nighttime light radiance data. POIs (points of interest, which are derived from an online mapping service https://maps.baidu.com/), which consist of residential, financial and commercial, shopping, transportation and agricultural service sites, are used to investigate variations in socioeconomic activities among different types of partitioned sub-regions.

2.3. Watershed-Based Partition of VIIRS Images

Without the effect of lighting saturation, VIIRS images enable us to obtain detailed observations of anthropogenic nocturnal radiances with visible spatial fluctuations at a fine scale (see Figure 2a). Local variations in nighttime lighting signals, however, are still affected by the over-glow effect at the grid cell-level [34]. As illustrated in Figure 2b, even though grid cell A and grid cell B have approximately the same NTL, they could have distinctly different information regarding local anthropogenic lighting at night. Grid cell B cannot be directly regarded as an independent light source due to the local high brightness level in neighboring grid cell D and the potential influence of radiance in grid cell B. In contrast, the over-glow effect from grid cell D is unlikely to reach grid cell A because local minimum nighttime brightness is occurring in grid cell C (between A and D). Both grid cell A and D exhibit local maximum brightness and can therefore be treated as local hotspots for nighttime light radiance; these hotspots are connected to independent anthropogenic lighting sources, which are detectable by the VIIRS monthly DNB image at the pixel level.

At the regional scale, spatially distributed local hotspots of nighttime lighting develop fundamental spatial patterns in human settlements consisting of various socioeconomic activities; this method shows the distinct magnitudes of nocturnal artificial lighting areas that are observed in VIIRS images. Even though we are unable to create the link between local hotspots and exact artificial objects on the ground due to the limited spatial resolution of current nightlight images, nocturnal lighting hotspots represent local centers of aggregated demographic and socioeconomic activities across a given human settlement and, thus, enable us to spatially partition the region into different sub-regions with locally independent nighttime lighting sources, which respond to diverse human activities at the local scale. In this study, we used a watershed transformation to separate adjacent sub-regions around identified local hotspots of nighttime lighting [42]. The watershed transformation operates upon a VIIRS image, such as a topographic map, where the nighttime radiance of each grid cell corresponds to its height (Figure 2c) and outlines the boundaries that run along the bottoms of the valleys (the opposite of traditional catchment basins, which are outlined by the tops of ridges). As shown in Figure 2d, each nightlight watershed unit contains a local hotspot of nighttime lighting, which is surrounded by adjacent grid cells whose radiance values do not exceed its own;

the boundary of the unit is the periphery of the local minimum nighttime brightness, which is shared with neighboring nightlight watershed units.

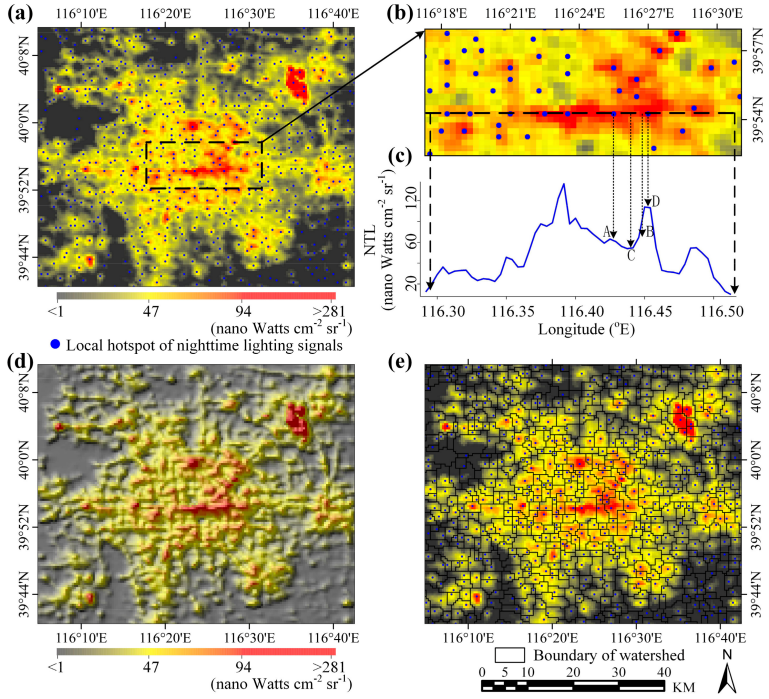

Figure 2. Illustrations of the watershed-based partition method. (**a**) VIIRS nighttime radiances and local hotspots of lighting signals in the city of Beijing; (**b**) Spatial variations in VIIRS nighttime light (NTL); (**c**) The profile of NTL across a longitudinal transect; (**d**) A topographic map of nighttime light; (**e**) Spatial divisions partitioned by the watershed-based approach.

2.4. The Second Order Exponential Decay Model

The nighttime light watershed approach provides primary spatial divisions to delineate patterns in human settlements. Apart from the spatial resolution of nighttime light images, the partitioned result is mainly determined by the type of human settlement related to the spatial variations in local human activity. In general, increased spatial heterogeneity in human activity for a diversely populated human settlement, particularly across rural–urban gradients with distinct urbanization levels, can yield an increase in various nightlight watershed divisions with different extents and underlying degrees of human activities (Figure 3a). As shown in Figure 3b, we find that the quantitative relationship between the individual rank in nighttime brightness and the corresponding NTL among local hotspots exhibits a significant second order exponential decay over the whole region. The second order exponential decay model formula can be expressed as:

$$\mathrm{NTL}(rank) = A_1 \times exp^{\left(-\frac{rank}{\mathrm{Rank}_1}\right)} + A_2 \times exp^{\left(-\frac{rank}{\mathrm{Rank}_2}\right)} \quad (1)$$

where A_1 and A_2 are the fitting coefficients, *rank* is the descending order label for a given grid cell with NTL, Rank_1 and Rank_2 represent the short and long transition spans of the human activity spatial dynamics for the fast process along the urban–rural gradient (from left to right in Figure 3b) and the slow process along the rural–urban gradient (from right to left in Figure 3b), respectively.

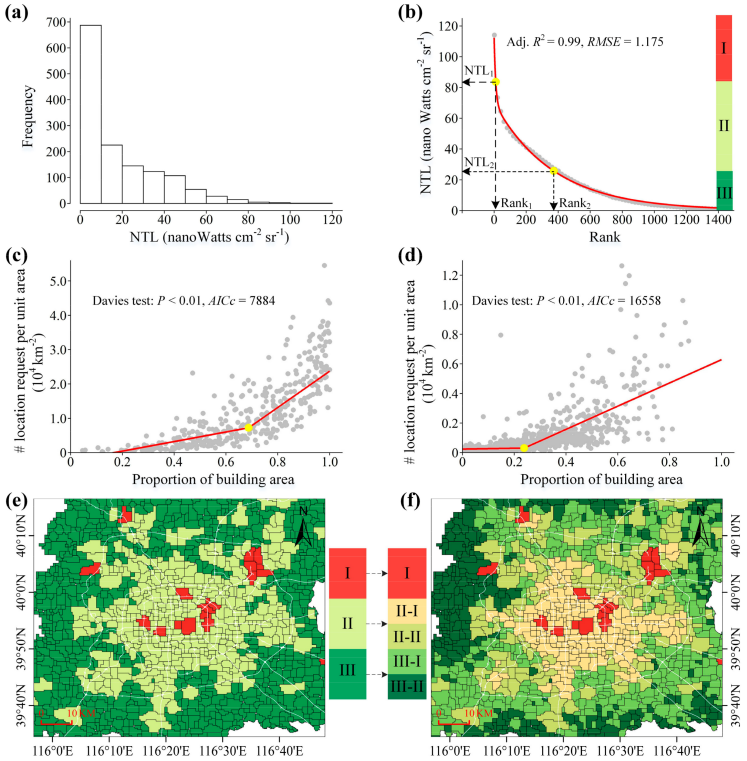

Figure 3. (**a**) Statistical histogram of VIIRS NTL distributions at the watershed division level in the city of Beijing; (**b**) The relationship between individually ranked nightlight regions and corresponding NTL according to the second order exponential decay model; (**c**) Segmented bivariate linear fit for type II watershed nightlight divisions; (**d**) Segmented bivariate linear fit for type III watershed nightlight divisions; Yellow dots in both (**c**,**d**) represent turning points determined by a piecewise regression. (**e**) Spatially partitioned results according to (**b**); (**f**) Spatially partitioned results according to (**b**–**d**).

The second order exponential decay of the rank-NTL distribution for local nighttime brightness, with a long concave-upward tail, can be attributed to the spatial distribution of human activities, which is characterized by a gradual decay in local maximum NTL from the urbanized area throughout the peripheral and rural areas, where an increased amount of sub-regions across the whole human settlement shows a right-skewed distribution of local maximum NTL (Figure 3a). By fitting Equation (1), we can obtain two key radiance thresholds NTL_1 and NTL_2 for identifying transition spans of human activity in partitioned nightlight units (see Figure 3b). Hence, paired values of $Rank_1$–NTL_1 and $Rank_2$–NTL_2, which are derived from the second order exponential decay, provide a primary classification of nightlight watersheds with three different types: I (VIIRS radiance range > NTL_1), II (range from NTL_2 to NTL_1) and III (range < NTL_2) nighttime lighting areas. It should be noted that there could be regionally high lighting divisions that typically cover the airport, the large central business district and the high density residential area. These divisions can be determined though NTL_1 with the second order exponential decay model for agglomerations (Jing-Jin-Ji in this case). We excluded these divisions from the regression fitting and classified them as type I to reduce the effect of the regional upper outliers in lighting divisions on the of the second order exponential decay model (with an exceptionally fast decay) at the local scale.

2.5. Further Identification Based on the Bivariate Relationship

Both type II and III nightlight watersheds can be further partitioned into several subtypes with the aid of two additional variables, including the proportion of the building area (defined as the ratio between the GUF-derived building area and the grid cell area) and the degree of human activity

(calculated as the total number of Tencent-derived location requests per unit area). In the bivariate plot (Figure 3c,d), we can estimate the positive response of the degree of human activity to the proportion of building areas with a step change. Thus, we used a piecewise regression model with two line segments to fit the quantitative relationship among nightlight watersheds, separately, for types II and III in order to determine the turning point in the bivariate plot (as represented by yellow dots in Figure 3c,d). The turning value for the proportion of building areas was employed to further partition type II and III nightlight watershed divisions into II-I and II-II and III-I and III-II, respectively.

Based on the VIIRS nighttime light image associated with building and human activity data, we obtain a total of five types of spatially partitioned nightlight watershed divisions: I, II-I, II-II, III-I and III-II. Comparing the partitioning result with all initial images, as shown in Figure 1, we can empirically find that (1) type I nightlight watersheds, with a regionally high number of lighting areas, likely cover transportation hubs, the central business district and the high density residential area; (2) type II-I nightlight watersheds, with high-medium lighting and human activity areas, typically represent developed urban land with intense human activities and a high percentage of buildings; (3) type II-II nightlight watersheds, with medium lighting and human activity areas, appear to cover the periphery of the urbanized area, which has a considerable amount of artificial buildings and human activities; (4) type III-I nightlight watersheds, with medium-low lighting and human activity areas, can be linked to suburban areas; and (5) type III-II nightlight watersheds, with low lighting and human activity areas, primarily cover rural areas, including small towns, villages, rural residential sites and other remote lands.

3. Results and Discussion

3.1. Comparisons of Different Types of Nighttime Lighting Areas

We used classified POIs data to examine whether different types of nightlight watershed areas can be connected to various human activities. As demonstrated in the city of Beijing, all POIs across the region are categorized into five subgroups: residential, financial, shopping, transportation and agricultural. We statistically test the null hypothesis regarding the proportion of subgroup POIs (accounting for all types of POIs) in a given type of nightlight watershed division and for the whole city (two-sided with a Yates' continuity correction). Table 1 lists the ratios of the proportioned and sub-grouped POIs between nightlight watershed divisions and the NTL regions and their corresponding significance test results for all five subgroups of POIs across five types of nightlight watershed divisions. A ratio greater than 1 indicates that the nightlight watershed division has a relatively higher proportion of given POIs than that for the whole city, and vice versa.

Table 1. Summary of the proportional test for various types of points of interest (POIs) across different kinds of watershed lighting division in Beijing City according to the partition result shown in Figure 3.

Type		Residential	Financial	Shopping	Transportation	Agricultural
I	High	0.74^{---}	1.24^{+++}	1.50^{+++}	0.89^{--}	0.06^{---}
II-I	High-medium	1.04^{+++}	1.04^{+++}	0.88^{---}	0.87^{---}	0.11^{---}
II-II	Medium	1.18^{+++}	0.81^{---}	0.97	1.09^{++}	1.26^{+++}
III-I	Medium-low	0.82^{---}	0.67^{---}	1.14	2.16^{+++}	6.59^{+++}
III-II	Low	0.65^{---}	0.90	0.93	0.76^{-}	14.35^{+++}

$^{+++}$ Greater with $p < 0.001$; $^{++}$ greater with $p < 0.05$; $^{---}$ less with $p < 0.001$; $^{--}$ less with $p < 0.05$; $^{-}$ less with $p < 0.1$.

Based on the analysis results from the proportion testing summarized in Table 1, we can find distinct connections between different types of partitioned nighttime lighting areas and diverse types of POIs, which might indicate a regionally regular distribution of underlying various human activities across human settlements. In general, both high-medium and medium lighting areas have a relatively high proportion of residential sites, while both high and low lighting areas show a low proportion of residential sites. High density financial sites and shopping sites appear to occur in high to high-medium lit areas and high brightness areas, respectively, with relatively intensified human

activity. Medium-low lighting areas exhibit a distinctive high proportion of transportation-related sites. It is also expected that a major proportion of agricultural activity-related sites occurs in low and medium-low lighting areas.

3.2. City-Level Characteristics of Nightlight Partitions

We performed spatial partitions of VIIRS images using a watershed-based approach for 99 city-level regions in 10 major urban agglomerations in China. Figure 4 represents the statistical relationships among several variables employed in the watershed-based partition of VIIRS nighttime light images over 99 cities. Maps of the spatial partition results for 10 urban agglomerations are shown in Figure 5. As shown in Figure 4a, NTL_1 and NTL_2, which are derived from the second order exponential decay model, show a positive linear relationship across all target cities. This result indicates that there is not a single threshold for nighttime brightness that is widely applicable for identifying different types of watershed lighting divisions across various regions with VIIRS images. At the city-level, artificial nighttime lighting signals, which are typically connected to a certain degree of local human activity, may vary with the size and form of the human settlement with a distinct socioeconomic status and urbanization levels. Moreover, the regional total lit area in the VIIRS images shows a rapid increase with the enhanced artificial building area according to the log-linear model (Figure 4b). This result could imply an accelerated increase in the spatial extent of lit areas, which simultaneously responds to the concurrent development of human settlements. Visible variations in the turning point of the bivariate piecewise regression (Figure 4c,d) further demonstrate the regional differences in human activity in terms of the relationship between these two socioeconomic variables. Overall, large cities (e.g., Beijing and Shanghai in Figure 4b) typically show relatively high thresholds of nighttime radiance (Figure 4a) and socioeconomic variables (Figure 4c,d) for different types of spatial partitions regarding human settlements due to increased responses in the observed variables depending on the size of the city. Small and medium-sized individual cities could have relatively high NTL thresholds (e.g., Benxi and Fushu in Figure 4a) or turning values (e.g., Putian in Figure 4d) largely because the city is generally dominated by industrial or commercial services.

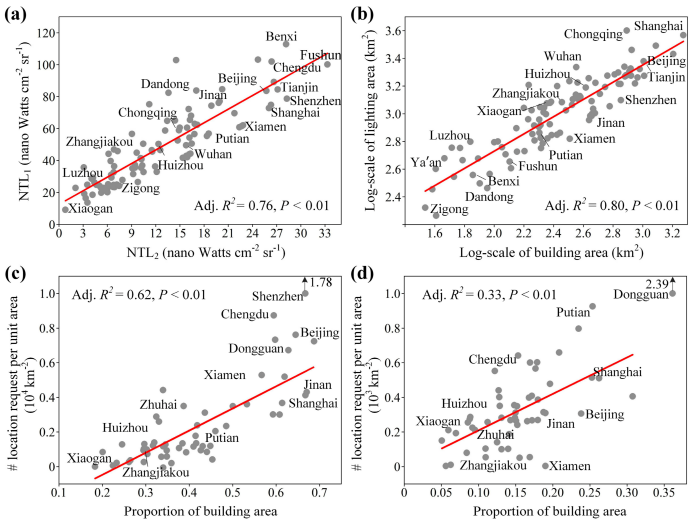

Figure 4. Statistical analyses of watershed-based partitions from VIIRS nighttime images across cities in 10 of China's major urban agglomerations. (**a**) NTL_1 against NTL_2 for 99 cities (see Equation (1) and Figure 2b for definitions); (**b**) Log-linear relationship between lit areas and building areas, excluding type III-II nightlight watersheds for 99 cites; (**c**) The turning value of the bivariate regression for partitions of type II nightlight watersheds (as illustrated in Figure 3c) across 56 cities with $p < 0.01$ by Davies test in segmented regression as shown in Figure 3; (**d**) The turning value of the bivariate regression for partitions of type III nightlight watersheds (as illustrated in Figure 3d) across 54 cites with $p < 0.01$ by Davies test.

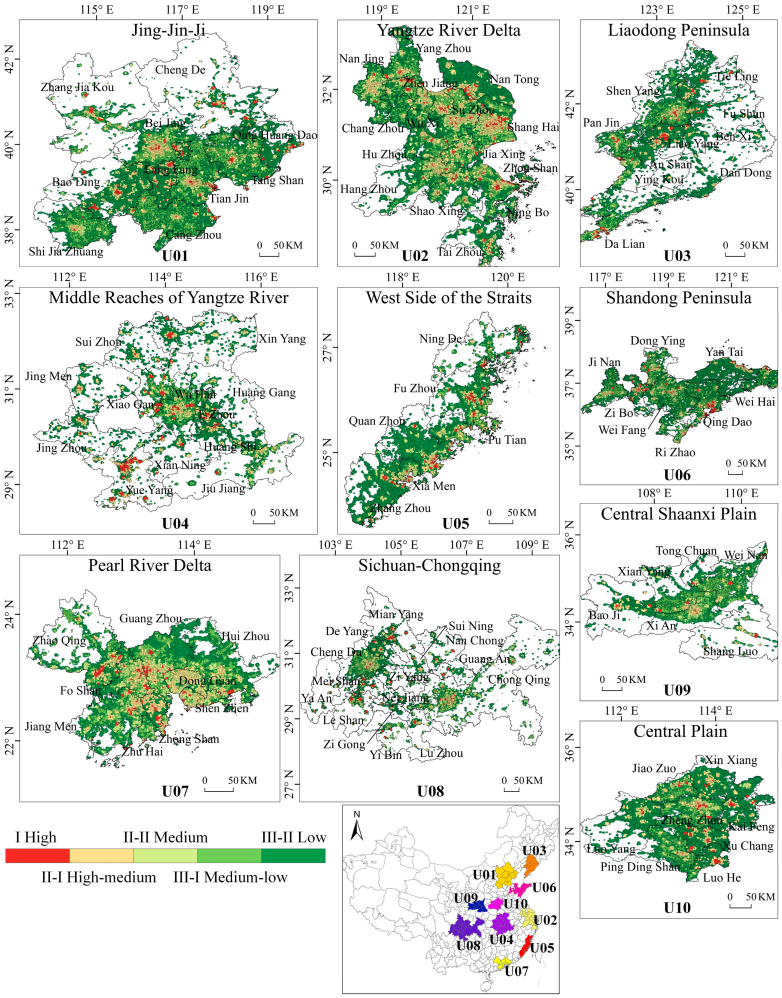

Figure 5. VIIRS image-derived spatial partition results of human settlements for 99 cities in 10 major urban agglomerations in China using the watershed-based approach.

3.3. Regional-Level Patterns of Human Settlement

A watershed-based partition of VIIRS images allows us to obtain a spatially explicit distribution of different types of nighttime lighting divisions associated with various magnitudes of human activity across human settlements over 10 urban agglomerations (see Figure 5). High-density lighting areas disperse over the region and constitute local centers of diverse human activities. High-medium lighting divisions surrounding local hotspots of human activity generally cover major built-up areas and pass through the administrative boundaries of cities, particularly in large urban clusters (e.g., the Yangtze River Delta and the Pearl River Delta), which are linked by continuously urbanized areas. Medium lighting areas appear to occur in both suburban zones and small cities or large townships, while low lighting areas mainly occur in rural areas. Moreover, we performed the proportional test of various types of POIs for I and II-III partitioned units across 10 urban agglomerations. Analysis results (as listed in Appendix A Table A1) show notable differences in relative proportions of various types of POIs with respect the whole region between these two kinds of partitioned units.

On average and only accounting for nearly 10% of the total lighting areas, high and high-medium density lighting areas hold more than 30% of the artificial buildings and over half of the location requests (see Figure 6). Moreover, there are also inter-regional variations in the relative proportion of lighting areas, building areas and the total number of location requests among different types of partitioned lighting divisions in the 10 agglomerations. Both the urban agglomerations of Jing-Jin-Ji and the Middle Reaches of Yangtze River show relatively higher proportioned areas, with above

medium density lighting and human activity areas. The former is largely due to the sizable urbanized area, and the latter is likely due to less rural area that is limited by the mountainous terrain. Relatively high percentages of both building areas and the number of location requests that occur in high density lighting divisions are typically found along the West Side of the Straits, Sichuan-Chongqing and the Central Shaanxi Plain, which indicates a moderate concentration of human activity in these regions. Even though there are notable levels of urbanization and socioeconomic activities, both the Yangtze River Delta and the Pearl River Delta commonly show a relatively low percentage of above medium density lighting and human activity areas, as well as relatively low concentrations of both building areas and the number of location requests. The Liaodong Peninsula, the Shandong Peninsula and the Central Plain show a regional dispersion of above medium density human activity regions due to the relatively low magnitudes of urbanization and socioeconomic activities in these regions.

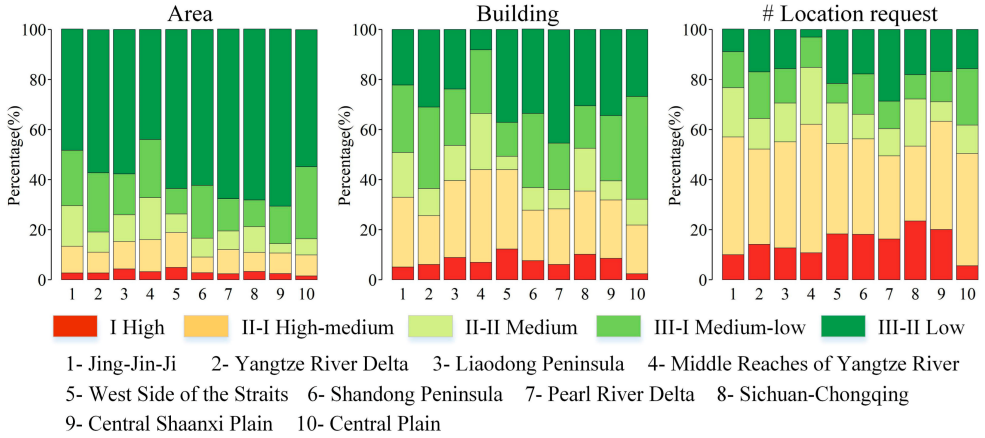

Figure 6. Comparisons of relative lighting areas (**left**), building areas (**middle**) and the total number of location requests (**right**) among different types of partitioned lighting divisions across 10 major urban agglomerations in China.

4. Conclusions

Timely and consistent observations of artificial lighting areas at night provide a unique data source for investigating urbanization dynamics and socioeconomic activities across human settlements in a spatially explicit manner [43]. The fundamental aspects of satellite-derived nighttime light data regarding their application are positive and monotonic responses (e.g., linear, exponential and power-law functions) of total nighttime brightness or lit areas to corresponding demographic and socioeconomic variables at the local and regional scales [44–46]. A reduction in texture information regarding artificial objects in nighttime light images is still a major challenge when delineating the spatial patterns in human settlements using nocturnal luminosity data, even for VIIRS images with markedly enhanced spatial resolutions and less over-glow effects than those of traditional DMSP images [34].

Based on the local hotspots of lighting signals and the spatial fluctuations in nighttime brightness, we developed a watershed-based partition approach for VIIRS images. This method is used to separate adjacent sub-regions like a topographic map. NTL thresholds, which can be used for the further classification of partitioned watershed divisions, are developed by a second order exponential decay model, which can outline the spatial transitions in nighttime radiances along both rural–urban and urban–rural gradients. Using satellite-derived building densities and social media-derived human activity data, we finally obtained a classification of watershed lighting divisions, including five types of high, high-medium, medium, medium-low and low-density lighting and human activity areas across the human settlement. Different types of partitioned and classified areas can be connected to distinct human activities through quantitative comparisons of the relative proportions of different

types of POIs (points of interest). Moreover, we find that NTL thresholds for the partitioning of VIIRS images are inter-regionally various and likely depend on the size and form of the human settlement. Thus, nightlight image-based investigations of human settlement patterns should vary according to the features of the target region, even for VIIRS data with a high spatial resolution and few over-glow and saturation effects. In addition, our results suggest that the association of nighttime light data with geo-located social median data should further benefit our understanding of patterns in human settlement with enhanced human activity information.

Our watershed-based partition method can provide insight into the application of VIIRS nighttime light images when spatially characterizing the various patterns and degrees of human activity across the human settlement. It is noteworthy that our method uses a watershed lighting area as an analysis unit and, hence, several details regarding local human activity might be ignored. Therefore, a pixel-based partition method that considers the pixel-level response of nighttime radiance signals to local human activity at a fine scale is essential and should be investigated in order to promote future applications of VIIRS nighttime light data to urbanization and socioeconomic dynamics with spatially explicit details.

Acknowledgments: This study was funded by the Key Research Program of Frontier Science, Chinese Academy of Sciences (No. QYZDY-SSW-DQC007), the National Natural Science Foundation of China (No. 41771418, 41421001), the National Science and Technology Key Project (No. 2016YFB0502301) and the National Key Basic Research Program of China (No. 2015CB954101).

Author Contributions: T.M. conceived and designed the study and methods; Z.Y. and A.Z. performed the experiments; T.M., Z.Y. and A.Z. analyzed the data; T.M. wrote the paper.

Conflicts of Interest: The authors declare no conflict of interest.

Appendix A

Table A1. Summary of the proportional test of various types of POIs for kinds of I and III-II watershed lighting division across 10 urban agglomerations as shown in Figure 5.

Region	Type	Residential	Financial	Shopping	Transportation	Agricultural
U01	I	1.14^{+++}	1.27^{+++}	1.49^{+++}	0.80^{---}	0.14^{---}
	III-II	0.19^{---}	0.31^{---}	0.31^{---}	1.45^{+++}	4.52^{+++}
U02	I	1.22^{+++}	1.32^{+++}	1.37^{+++}	1.12^{+++}	0.33^{---}
	III-II	0.22^{---}	0.78^{---}	0.49^{---}	0.77^{---}	5.27^{+++}
U03	I	0.88^{---}	1.27^{+++}	1.33^{+++}	1.12^{+++}	0.11^{---}
	III-II	0.26^{---}	0.41^{---}	0.31^{---}	0.33^{---}	5.62^{+++}
U04	I	1.22^{+++}	1.07^{+++}	1.27^{+++}	1.10^{+++}	0.13^{---}
	III-II	0.23^{---}	0.89^{---}	0.61^{-}	0.43^{---}	4.03^{+++}
U05	I	1.30^{+++}	1.01	0.81^{---}	0.95^{---}	0.41^{--}
	III-II	0.23^{---}	1.03	0.63^{---}	0.87^{---}	3.42^{+++}
U06	I	1.00	1.19^{+++}	1.11^{+}	1.20^{+++}	0.16^{--}
	III-II	0.52^{---}	0.66^{---}	0.45^{---}	0.48^{---}	3.51^{+++}
U07	I	1.27^{+++}	1.07^{+++}	0.60^{---}	1.06^{+++}	0.00^{---}
	III-II	0.31^{---}	0.77^{---}	1.10^{+}	0.81^{---}	8.02^{+++}
U08	I	1.11^{+++}	1.06^{+++}	1.41^{+++}	0.81^{---}	0.30^{---}
	III-II	0.39^{---}	0.78^{---}	0.36^{---}	0.80^{---}	3.85^{+++}
U09	I	0.95	1.32^{+++}	1.53^{+++}	0.89^{---}	0.00
	III-II	0.31^{---}	0.74^{---}	0.47^{---}	1.13^{+++}	8.23^{+++}
U10	I	1.15^{+++}	1.19^{+++}	1.27^{+++}	0.96^{---}	0.26^{---}
	III-II	0.12^{---}	0.40^{---}	0.44^{---}	0.83^{---}	1.93^{+}

$^{+++}$ Greater with $p < 0.001$; $^{+}$ greater with $p < 0.1$; $^{---}$ less with $p < 0.001$; $^{--}$ less with $p < 0.05$; $^{-}$ less with $p < 0.1$. U01-Jing-Jin-Ji; U02-Yangtze River Delta; U03-Liaodong Peninsula; U04-Middle Reaches of Yangtze River; U05-West Side of the Straits; U06-Shandong Peninsula; U07-Pearl River Delta; U08-Sichuan-Chongqing; U09-Central Shannxi Plain; U10-Central Plains.

References

1. Grimm, N.B.; Faeth, S.H.; Golubiewski, N.E.; Redman, C.L.; Wu, J.; Bai, X.; Briggs, J.M. Global change and the ecology of cities. *Science* **2008**, *319*, 756–760. [CrossRef] [PubMed]
2. Alberti, M. The effects of urban patterns on ecosystem function. *Int. Reg. Sci. Rev.* **2005**, *28*, 168–192. [CrossRef]
3. Goudie, A.S. *The Human Impact on the Natural Environment: Past, Present, And Future*; John Wiley & Sons: Hoboken, NJ, USA, 2013.
4. Jenerette, G.D.; Harlan, S.L.; Brazel, A.; Jones, N.; Larsen, L.; Stefanov, W.L. Regional relationships between surface temperature, vegetation, and human settlement in a rapidly urbanizing ecosystem. *Landsc. Ecol.* **2007**, *22*, 353–365. [CrossRef]
5. Pauleit, S.; Ennos, R.; Golding, Y. Modeling the environmental impacts of urban land use and land cover change—A study in Merseyside, UK. *Landsc. Urban Plan.* **2005**, *71*, 295–310. [CrossRef]
6. Milesi, C.; Elvidge, C.D.; Nemani, R.R.; Running, S.W. Assessing the impact of urban land development on net primary productivity in the southeastern United States. *Remote Sens. Environ.* **2003**, *86*, 401–410. [CrossRef]
7. Ghosh, T.; Elvidge, C.; Sutton, P.C.; Baugh, K.E.; Powell, R.; Anderson, S. Shedding light on the global distribution of economic activity. *Open Geogr. J.* **2010**, *3*, 148–161.
8. Elvidge, C.D.; Baugh, K.E.; Kihn, E.A.; Kroehl, H.W.; Davis, E.R.; Davis, C.W. Relation between satellite observed visible-near infrared emissions, population, economic activity and electric power consumption. *Int. J. Remote Sens.* **1997**, *18*, 1373–1379. [CrossRef]
9. Xu, T.; Ma, T.; Zhou, C.; Zhou, Y. Characterizing spatio-temporal dynamics of urbanization in China using time series of DMSP/OLS night light data. *Remote Sens.* **2014**, *6*, 7708–7731. [CrossRef]
10. Small, C.; Elvidge, C.D. Mapping decadal change in anthropogenic night light. *Procedia Environ. Sci.* **2011**, *7*, 353–358. [CrossRef]
11. Bennett, M.M.; Smith, L.C. Advances in using multitemporal night-time lights satellite imagery to detect, estimate, and monitor socioeconomic dynamics. *Remote Sens. Environ.* **2017**, *192*, 176–197. [CrossRef]
12. Zhang, Q.; Seto, K.C. Mapping urbanization dynamics at regional and global scales using multi-temporal DMSP/OLS nighttime light data. *Remote Sens. Environ.* **2011**, *115*, 2320–2329. [CrossRef]
13. Elvidge, C.D.; Baugh, K.E.; Kihn, E.A.; Kroehl, H.W.; Davis, E.R. Mapping city lights with nighttime data from the DMSP Operational Linescan System. *Photogramm. Eng. Remote Sens.* **1997**, *63*, 727–734.
14. Elvidge, C.D.; Cinzano, P.; Pettit, D.; Arvesen, J.; Sutton, P.; Small, C.; Nemani, R.; Longcore, T.; Rich, C.; Safran, J. The Nightsat mission concept. *Int. J. Remote Sens.* **2007**, *28*, 2645–2670. [CrossRef]
15. Huang, Q.; Yang, X.; Gao, B.; Yang, Y.; Zhao, Y. Application of DMSP/OLS nighttime light images: A meta-analysis and a systematic literature review. *Remote Sens.* **2014**, *6*, 6844–6866. [CrossRef]
16. Cao, X.; Chen, J.; Imura, H.; Higashi, O. A SVM-based method to extract urban areas from DMSP-OLS and SPOT VGT data. *Remote Sens. Environ.* **2009**, *113*, 2205–2209. [CrossRef]
17. Henderson, M.; Yeh, E.T.; Gong, P.; Elvidge, C.; Baugh, K. Validation of urban boundaries derived from global night-time satellite imagery. *Int. J. Remote Sens.* **2003**, *24*, 595–609. [CrossRef]
18. Zhang, Q.; Schaaf, C.; Seto, K.C. The vegetation adjusted NTL urban index: A new approach to reduce saturation and increase variation in nighttime luminosity. *Remote Sens. Environ.* **2013**, *129*, 32–41. [CrossRef]
19. Hillger, D.; Kopp, T.; Lee, T.; Lindsey, D.; Seaman, C.; Miller, S.; Solbrig, J.; Kidder, S.; Bachmeier, S.; Jasmin, T. First-light imagery from Suomi NPP VIIRS. *Bull. Am. Meteorol. Soc.* **2013**, *94*, 1019–1029. [CrossRef]
20. Elvidge, C.D.; Baugh, K.E.; Zhizhin, M.; Hsu, F.-C. Why VIIRS data are superior to DMSP for mapping nighttime lights. *Proc. Asia-Pac. Adv. Netw.* **2013**, *35*, 62–69. [CrossRef]
21. Levin, N. The impact of seasonal changes on observed nighttime brightness from 2014 to 2015 monthly VIIRS DNB composites. *Remote Sens. Environ.* **2017**, *193*, 150–164. [CrossRef]
22. Falchi, F.; Cinzano, P.; Duriscoe, D.; Kyba, C.C.; Elvidge, C.D.; Baugh, K.; Portnov, B.A.; Rybnikova, N.A.; Furgoni, R. The new world atlas of artificial night sky brightness. *Sci. Adv.* **2016**, *2*, e1600377. [CrossRef] [PubMed]
23. Ma, T.; Zhou, C.; Tao, P.; Haynie, S.; Fan, J. Responses of Suomi-NPP VIIRS-derived nighttime lights to socioeconomic activity in China's cities. *Remote Sens. Lett.* **2014**, *5*, 165–174. [CrossRef]

24. Small, C.; Elvidge, C.D.; Baugh, K. Mapping urban structure and spatial connectivity with VIIRS and OLS night light imagery. In Proceedings of the 2013 Joint Urban Remote Sensing Event (JURSE), Sao Paulo, Brazil, 21–23 April 2013; pp. 230–233.
25. Li, X.; Xu, H.; Chen, X.; Li, C. Potential of NPP-VIIRS nighttime light imagery for modeling the regional economy of China. *Remote Sens.* **2013**, *5*, 3057–3081. [CrossRef]
26. Xie., Y.; Weng, Q.; Weng, A.; Xie., Y.; Weng, Q.; Weng, A. A comparative study of NPP-VIIRS and DSMP-OLS nighttime light imagery for derivation of urban demographic metrics. In Proceedings of the 2014 Third International Workshop on Earth Observation and Remote Sensing Applications (EORSA), Changsha, China, 11–14 June 2014; pp. 335–339.
27. Ma, T.; Zhou, Y.; Wang, Y.; Zhou, C.; Haynie, S.; Xu, T. Diverse relationships between Suomi-NPP VIIRS night-time light and multi-scale socioeconomic activity. *Remote Sens. Lett.* **2014**, *5*, 652–661. [CrossRef]
28. Shi, K.; Huang, C.; Yu, B.; Yin, B.; Huang, Y.; Wu, J. Evaluation of NPP-VIIRS night-time light composite data for extracting built-up urban areas. *Remote Sens. Lett.* **2014**, *5*, 358–366. [CrossRef]
29. Sharma, R.C.; Tateishi, R.; Hara, K.; Gharechelou, S.; Iizuka, K. Global mapping of urban built-up areas of year 2014 by combining MODIS multispectral data with VIIRS nighttime light data. *Int. J. Digit. Earth* **2016**, *9*, 1004–1020. [CrossRef]
30. Xie, Y.; Weng, Q. Updating urban extents with nighttime light imagery by using an object-based thresholding method. *Remote Sens. Environ.* **2016**, *187*, 1–13. [CrossRef]
31. Zhou, Y.; Smith, S.J.; Elvidge, C.D.; Zhao, K.; Thomson, A.; Imhoff, M. A cluster-based method to map urban area from DMSP/OLS nightlights. *Remote Sens. Environ.* **2014**, *147*, 173–185. [CrossRef]
32. Lu, D.; Tian, H.; Zhou, G.; Ge, H. Regional mapping of human settlements in southeastern China with multisensor remotely sensed data. *Remote Sens. Environ.* **2008**, *112*, 3668–3679. [CrossRef]
33. Imhoff, M.L.; Lawrence, W.T.; Stutzer, D.C.; Elvidge, C.D. A technique for using composite DMSP/OLS "city lights" satellite data to map urban area. *Remote Sens. Environ.* **1997**, *61*, 361–370. [CrossRef]
34. Dou, Y.; Liu, Z.; He, C.; Yue, H. Urban land extraction using VIIRS nighttime light data: An Evaluation of Three Popular Methods. *Remote Sens.* **2017**, *9*, 175. [CrossRef]
35. Ma, T.; Zhou, Y.; Zhou, C.; Haynie, S.; Pei, T.; Xu, T. Night-time light derived estimation of spatio-temporal characteristics of urbanization dynamics using DMSP/OLS satellite data. *Remote Sens. Environ.* **2015**, *158*, 453–464. [CrossRef]
36. Levin, N.; Kark, S.; Crandall, D. Where have all the people gone? Enhancing global conservation using night lights and social media. *Ecol. Appl.* **2015**, *25*, 2153–2167. [CrossRef] [PubMed]
37. Liu, Y.; Sui, Z.; Kang, C.; Gao, Y. Uncovering patterns of inter-urban trip and spatial interaction from social media check-in data. *PLoS ONE* **2014**, *9*, e86026. [CrossRef] [PubMed]
38. Roick, O.; Heuser, S. Location based social networks-definition, current state of the art and research Agenda. *Trans. GIS* **2013**, *17*, 763–784. [CrossRef]
39. Miller, S.D.; Hawkins, J.D.; Kent, J.; Turk, F.J.; Lee, T.F.; Kuciauskas, A.P.; Richardson, K.; Wade, R.; Hoffman, C. NexSat: Previewing NPOESS/VIIRS imagery capabilities. *Bull. Amer. Meteorol. Soc.* **2006**, *87*, 433–446. [CrossRef]
40. Esch, T.; Marconcini, M.; Felbier, A.; Roth, A.; Heldens, W.; Huber, M.; Schwinger, M.; Taubenböck, H.; Müller, A.; Dech, S. Urban footprint processor-fully automated processing chain generating settlement masks from global data of the TanDEM-X mission. *IEEE Geosci. Remote Sens. Lett.* **2013**, *10*, 1617–1621. [CrossRef]
41. Zhu, D.; Huang, Z.; Shi, L.; Wu, L.; Liu, Y. Inferring spatial interaction patterns from sequential snapshots of spatial distributions. *Int. J. Geogr. Inf. Sci.* **2018**, *32*, 783–805. [CrossRef]
42. Chen, Z.; Yu, B.; Song, W.; Liu, H.; Wu, Q.; Shi, K.; Wu, J. A new approach for detecting urban centers and their spatial structure with nighttime light remote sensing. *IEEE Trans. Geosci. Remote Sens.* **2017**, *55*, 6305–6319. [CrossRef]
43. Chen, X.; Nordhaus, W.D. Using luminosity data as a proxy for economic statistics. *Proc. Natl. Acad. Sci. USA* **2011**, *108*, 8589–8594. [CrossRef] [PubMed]
44. Amaral, S.; Câmara, G.; Monteiro, A.M.V.; Quintanilha, J.A.; Elvidge, C.D. Estimating population and energy consumption in Brazilian Amazonia using DMSP night-time satellite data. *Comput. Environ. Urban Syst.* **2005**, *29*, 179–195. [CrossRef]

45. Jing, X.; Shao, X.; Cao, C.; Fu, X.; Yan, L. Comparison between the Suomi-NPP Day-Night Band and DMSP-OLS for correlating socio-economic variables at the provincial level in China. *Remote Sens.* **2015**, *8*, 17. [CrossRef]
46. Zhou, Y.; Ma, T.; Zhou, C.; Xu, T. Nighttime light derived assessment of regional inequality of socioeconomic development in China. *Remote Sens.* **2015**, *7*, 1242–1262. [CrossRef]